

Microstructural Characterization of Ti-6Al-4V Alloy Fiber Laser Weldments



Chandan Kumar and Manas Das

Abstract The quality of fiber laser welded specimens of Ti-6Al-4V alloy plates in butt joint is examined. A special kind of fixture is designed and fabricated for providing shielding gas. The microstructural analysis at various positions within heat-affected zone and in fusion zone are explored and its microstructural morphologies are compared. Due to the chronological distribution of temperature gradient, a nonhomogeneous microstructure is developed from fusion zone to base metal zone. Various kinds of microstructural morphology of martensitic structure, i.e., α' martensite, massive α (α_m), and blocky α are found in fusion zone. Also, the variations in amount of α' martensite are found inside heat-affected zones. Maximum hardness is obtained in fusion zone due to the occurrence of higher quantity of α' martensitic structure.

Keywords Ti-6Al-4V alloy · Fiber laser · Welding · Microstructure · Hardness

1 Introduction

Titanium and their alloys are most copious and abundant structural material on the earth planet. Titanium alloys are available in different grades. On the basis of presence of various phases at room temperature, titanium alloy is classified as α alloy, near α , β alloy and bimodal phases $\alpha + \beta$ alloy. The bimodal microstructure having both $\alpha + \beta$ phases in Ti-6Al-4V alloy is mostly utilized in automobile and aircraft industries. Ti-6Al-4V alloy is also known as grade 5 and it is identified as a workhorse in aerospace and automobile industries [1]. During heating, at around $995^\circ \pm 20^\circ \text{C}$ temperature, Ti-6Al-4V alloy is converted into fully β phase known as β transition temperature (T_β). It holds great features such as moderate strength, reasonable

C. Kumar

Department of Mechanical Engineering, Lovely Professional University, Phagwara, Jalandhar, Punjab, India
e-mail: kumar.chandan2006@gmail.com

M. Das (✉)

Department of Mechanical Engineering, IIT Guwahati, Assam 781039, India
e-mail: manasdas@iitg.ac.in

© Springer Nature Singapore Pte Ltd. 2020

B. B. Biswal et al. (eds.), *Advances in Mechanical Engineering*, Lecture Notes in Mechanical Engineering, https://doi.org/10.1007/978-981-15-0124-1_43

corrosion resistance, and great potential for weight saving. The aluminum can be replaced by Ti-6Al-4V alloy when operating temperature surpasses from 1300 °C [2]. A successful lightweight structure is the result of an optimized combination of selected material, design, and manufacturing process. When the lightweight components are manufactured by titanium and its alloys, welding is the most appropriate joining technology available yet. Weldability of pure titanium (Ti) and its alloys are excellent. Ti-6Al-4V is highly weldable among all the various $\alpha + \beta$ alloys. This weldability can be attributed to forming the high strength and acceptable ductility of the weldments. Ti-6Al-4V is highly resistant to solidification cracking. In spite of its excellent weldability special precautions should be taken during the welding process to reduce welding defects.

Fusion welds are obtained by the application of high intense heat source and subsequent solidification of the molten metal. The physical and chemical changes occur during fusion welding process due to the interaction between the high intense energy sources and the base metal that affect the bead shape, microstructure, and the mechanical properties of the weldments. Energy balance is maintained by the heat flux from top surface and loss of heat by conduction and radiation. The molten pool is driven by surface and body forces. The driving force for movement of molten material is the surface tension force that acts on the top surface of weld pool and the buoyancy force over entire volume of melt pool.

Laser beam welding (LBW) process is one kind of fusion welding. LBW is an autogenous, non-conventional, and appropriate welding technique to join similar as well as dissimilar materials of titanium and their alloys [3]. In LBW heat source having high energy density is applied on the workpiece surface and some of the energy is reflected back and remaining energy is absorbed by the workpiece to be welded and is converted to heat energy. The popularity of LBW process is increased due to its ability to produce high-quality weldments, low distortion in weldments, narrower heat-affected zones, noncontact type process and precisely controlled over intense energy source, high speed, and good flexibility over welding process. The demand for LBW by the industries is increasing rapidly due to lower production cost, rapid production capability, minimum distortion, and high efficiency compared to other successful joining technologies. The disadvantage of LBW process in butt configuration is its difficulty to achieve excellent joint fit-up, which requires lower value of surface roughness of the edges to be welded. When using laser for welding purposes, energy is transferred from the laser to the workpiece through two different ways or modes. The laser welding mode can be either the conduction mode or the keyhole mode depending upon the power density. In conduction mode, the low energy density basically heats the surface of the material being welded. The size of the weld on the surface is generally larger, and the depth of penetration of the weld is generally shallower. In conduction mode, power densities lie below 10^5 W/cm². In keyhole mode laser operation, the power density goes beyond the power density required for conduction mode. In keyhole mode, the local vaporization of base material takes place and a narrow vapor cavity is formed known as keyhole. This keyhole is surrounded by a thin layer of molten material and it is maintained by vapor pressure, surface tension force, and hydrostatic pressure. Keyhole mode of laser welding is mostly used

due to its capability to join thick sheets, high energy coupling efficiency, and faster welding speed. The conduction mode is also beneficial to minimize the distortion in the weldments and it reduces the chances of loss of alloying elements. Conduction mode of welding is highly recommended for joining of thin sheets due to the smaller spot diameter of laser beam which is comparable to the sheet thickness. The shape of weld bead is hemispherical in conduction mode of LBW process. Due to the rapid heating and cooling cycles in LBW, it yields fine grains in fusion zone and it improves the strength of the joint.

There are several kinds of laser, i.e., diode laser, carbon dioxide laser, neodymium-doped yttrium aluminum garnet laser, and fiber laser. Fiber laser is a high power density, flexible, and lower heat input process. It is a promising alternative to the conventional solid-state laser system. The fiber laser is widely used in industries and different areas of science and technology. It is mainly used in laser drilling, welding, marking, and cutting purpose. The use of fiber laser was started from early 1960s as a new welding heat source. In 2000, first 100 W and in 2005 maximum power of 17 kW fiber laser was produced. Also, newer technologies are coming up to produce high power fiber lasers. Fiber laser is preferred while welding of thick plates at high speed where conventional welding technique cannot be applied. In case of fiber laser, the active gain medium is optical fiber. The gain medium is doped with erbium, neodymium, dysprosium, ytterbium, etc. and it is excited by a diode laser. The outer cladding is enclosed with glass or polymeric material of low refraction coefficient to reduce the signal attenuation. The wall-plug efficiency of ytterbium-doped fiber laser is in between 16 and 20% which is higher than the erbium and thulium-doped fiber. However, it is more efficient than solid-state Nd: YAG laser. Fiber LBW gained great popularity because of high energy density, low line energy, higher efficiency, high beam quality, and lesser functional cost. Assuncao et al. [4] reported that fiber LBW offers extremely high welding speed and lowest operating cost per hour as compared to traditional laser. The main LBW process parameters are laser beam spot diameter, beam power, traverse speed, and flow rate of shielding gas [5]. Apart from these important process parameters, there are other factors which affect the quality of welded component as presented in Fig. 1.

A detailed study of the LBW processes on the basis of experimental and numerical works are addressed by various researchers. The microstructural analysis is studied by many researchers in the weldments of Ti-6Al-4V sheets by various kinds of lasers, i.e., CO₂ [6], Nd: YAG [7] and diode laser [8]. Gursel [9] reported that the high quality of weldments can be obtained at optimum welding conditions. An experimental investigation is carried out by Costa et al. [10] on the welding behavior of 6.5 mm thick Ti-6Al-4V sheets by fiber laser and stated that defect-free weld can be achieved under appropriate welding conditions. The welding defects are found at higher power and slower traverse speed. However, partial penetration is achieved in the workpiece combinedly at lower welding power and higher traverse speed. The welding experiments are carried out by Kabir et al. [11] on Ti-6Al-4V sheets by variation of traverse speeds and focal positions by means of Nd: YAG laser. On the basis of experimental results, they stated that the optimum value of defocused position and welding speed is required to attain high quality of weldments with acceptable

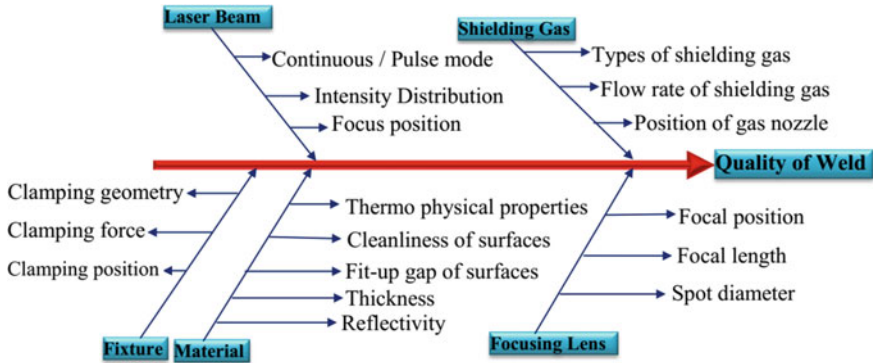


Fig. 1 LBW process parameters

welding defects. Casalino et al. [12] specified that the oxidation tendency of weldments is reduced by supplying the necessary amount of inert gas during Yb-doped fiber LBW of titanium alloy sheets. Also, the bead features are affected by heat input supplied on to the workpiece surfaces. Ahn et al. [13] found that beam power is a most significant parameter with respect to welding speed and defocussed distance in fiber LBW of Ti-6Al-4V plates for achieving high quality of weldments. Gao et al. [14] stated that lower line energy generates *V*-shaped bead while higher line energy creates *H*-shaped bead in Nd: YAG laser weldments of titanium alloy sheets. Also, they stated that *V*-shaped bead shows lower strength with respect to *H*-shaped bead.

It is found from the above literature assessment that the welding of titanium alloy by adopting fusion welding techniques is highly challenging and tough due to its higher reactivity with atmospheric gases above 300–500 °C temperature forming oxide layer and leads to weld defects in the weldments. Most of the LBW experiments on Ti-6Al-4V alloy are carried out by adopting CO₂ and solid-state Nd: YAG laser. However, limited works are reported on weld quality and bead characterization of Ti-6Al-4V alloy plates using newly developed fiber laser. In the current study, weldability of 1.5 mm thick Ti-6Al-4V plates is investigated using fiber laser in butt configuration. Also, the microstructural analysis is carried out at various locations within heat-affected zone (HAZ) and in fusion zone (FZ) using field emission scanning electron microscope (FESEM) and microstructural morphologies of FZ are analyzed and compared at different process parameters. Also, the relationship between hardness of the FZ and HAZ with microstructure evaluation in weld bead is discussed in details.

2 Experimentations

In this experimental study, A 2 kW multimode fiber laser heat source in continuous wave (CW) mode is used for laser welding experiments. The specification of fiber

Table 1 Description of fiber LBW machine

Working mode	CW
Spot diameter	200 μm
Wavelength	1.06 μm
Beam incident angle	85°
Shielding gas	Ar
Position of focal point	On the top surface

laser welding machine is shown in Table 1. Figure 2a depicts the fiber laser welding machine. The beam product parameter is less than 2.5 mm m-rad. The workstation is integrated with computer numerical control (CNC) system. The emission wavelength

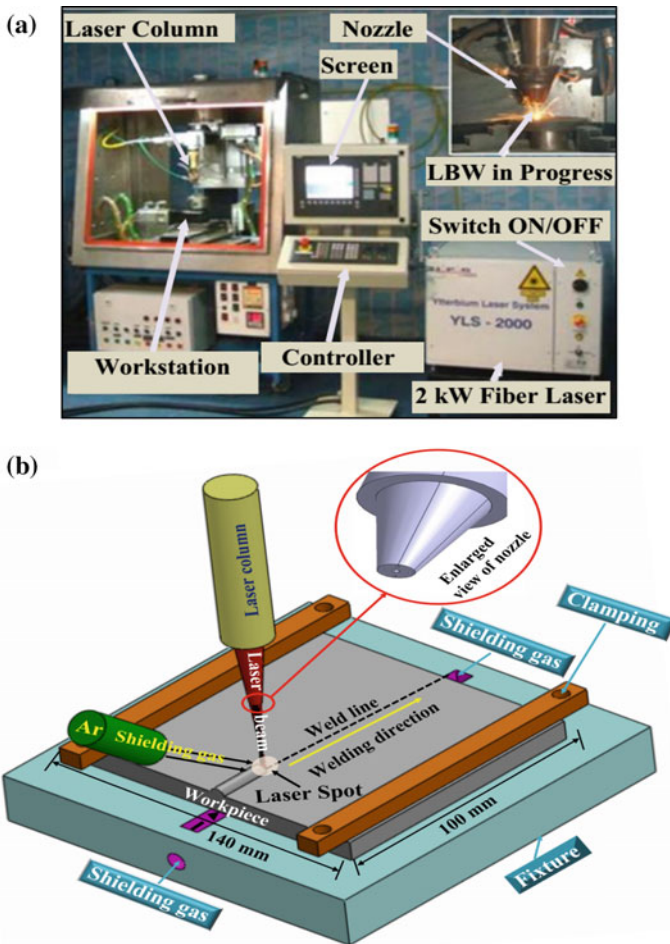


Fig. 2 a LBW welding set up b Fixture with shielding gas arrangement

Table 2 Composition of base metal (wt%)

Al	V	C	Si	O	Ti
5.8	4.2	0.08	0.2	0.21	Balance

is 1.06 μm and spot diameter on workpiece surface at “0” mm defocused position is 200 μm . The standoff distance of laser nozzle is 10 mm. The beam incident angle on workpiece surface is 85° and fiber core diameter is 50 μm . The elemental concentrations in the parent material of Ti-6Al-4V alloy are presented in Table 2. The workpiece dimension is $100 \times 70 \times 1.5 \text{ mm}^3$. The workpieces are carefully degreased by acetone swabbing prior to conduct the welding experiments to remove dust and iron particles, moisture, and grease. Otherwise iron particles may combine with titanium forming titanium–iron eutectic compound after solidification of molten metal which leads to cracks in the weldments. The joining edges of the specimens are made smooth in milling machine to minimize the gap between the specimens. The specimens are mounted on a specially designed workpiece fixture having provision to supply the shielding gas (Fig. 2b) to reduce the weld distortion and displacement during welding process.

During experiments, the shielding gas (i.e., argon) is provided from both sides of the workpiece fixture at a flow rate of 10 L per minute for protecting the trailing sides of the weld bead. Shielding gas is also supplied on the top surface of the specimen along the nozzle axis and from another nozzle which is inclined at 45° with the laser column at a flow rate of 5 L per minute (Fig. 2b) for bead shielding from atmospheric contamination. The welding experiments are conducted according to data provided in Table 3. The metallographic samples are prepared and polished by conventional method [15] and Kroll’s reagents are used as an etchant. Further, the hardness is measured by using Vickers microhardness testing equipment at load of 200 gf and dwell time of 15 s at an interval of 200 μm .

Table 3 Parameters for welding and bead observations

Exp. No.	Process variables			Observations
	P (W)	V (mm/min)	LE^a (J/mm)	
1	1100	500	132.05	Full penetration, underfill
2	1100	600	110	Full penetration
3	1100	700	94.26	Partial penetration, rejected

^aLE-line energy

3 Results and Discussion

3.1 Microstructure of Base Material (BM)

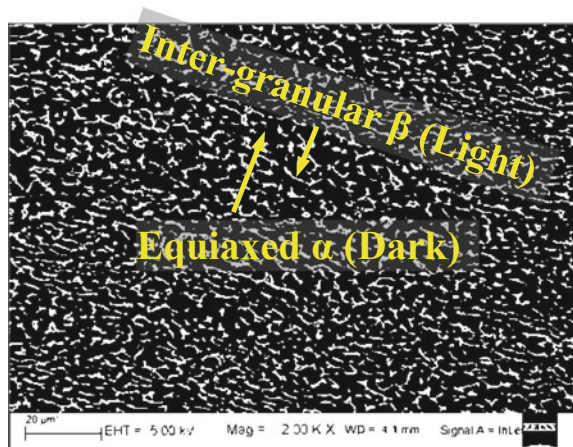
Microstructure (FESEM micrograph) of BM of Ti-6Al-4V plate is shown in Fig. 3. It consists of bimodal structure of equiaxed/elongated α (HCP structure) and intergranular β phases (BCC structure). The dark region in Fig. 3 indicates equiaxed α and light region indicates intergranular β phase.

3.2 Microstructure Within Heat-affected Zone (HAZ)

Figure 4a depicts the optical macrograph of weld bead of full penetration weldments of Exp. 2. Figures 4b–e show the FESEM images of microstructural changes inside HAZ at various positions, i.e., adjacent to FZ, center of HAZ, far away from FZ and nearby base metal zone (BMZ), respectively for Exp. 2. In the region of HAZ which is adjacent to FZ, maximum temperature goes beyond β transus temperature, i.e., T_β (995 °C for Ti-6Al-4V alloy) and remains below liquidus temperature, i.e., T_L (1655 °C). At this location, a combination of α' martensite and slightly lower quantity of blocky α is found as clearly shown in optical micrographs in Fig. 4b. Both the original α and β grains are not traced at this location inside HAZ.

Therefore, this location is named as fully transformed HAZ. At the center position of HAZ blocky α , original β , and a very less quantity of α' martensite is traced as depicted in Fig. 4c. The completely transformed HAZ is not traced at the center of HAZ because this location experiences lower peak temperature with respect to HAZ which is closer to FZ. The location in the HAZ far away from the FZ boundary made up of blocky type α and both primary α and primary β phases

Fig. 3 FESEM image of base metal microstructure



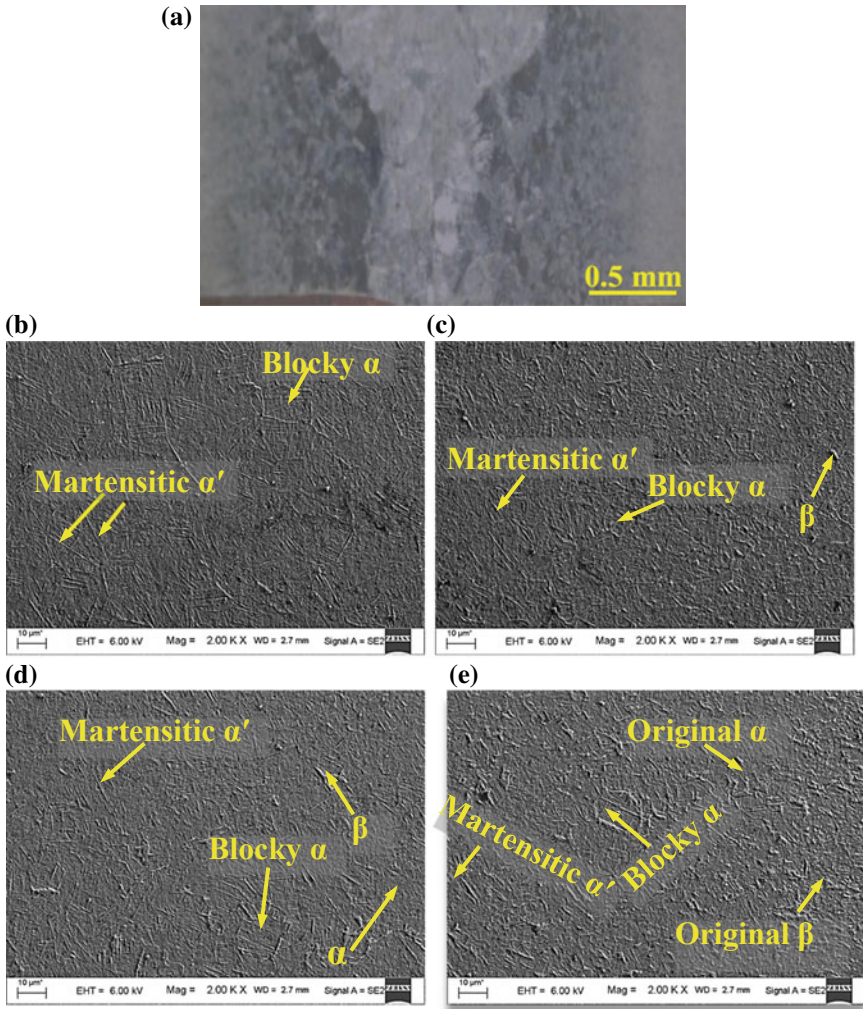


Fig. 4 **a** Optical macrograph of weld bead of full penetration weldments of Exp. 2; Microstructure within HAZ; **b** Adjacent to FZ, **c** Center of HAZ, **d** Far away from FZ, and **e** Nearby to BMZ for Exp. 2

and lesser volume of α' martensite as shown in Fig. 4d. In this region, the maximum temperature reaches below T_β and greater than the lowest temperature which is essential for microstructural modifications. This minimum temperature is very challenging to ascertain because it depends on transformation kinetics of the alloy. Similar microstructure is observed by Ahmed and Rack [16] while Ti-6Al-4V alloy was quenched below temperature range of 720–985 °C which is lesser than the T_β transition temperature of Ti-6Al-4V material. The microstructural features as shown

in FESEM images (Fig. 4e), in the HAZ which is near to BMZ are entirely different as compared to center of HAZ and near FZ. The region near to BMZ experiences lowest peak temperature with respect to other locations within HAZ. At this location, insignificant quantity of martensitic α' is traced in a dominant matrix of original α and β . Due to the incidence of higher quantity of original β and α phase, this area is named as partially transformed HAZ. From Fig. 4b–e, it is observed that the volume of α' martensite continuously reduces from around hundred percent in HAZ which is adjacent to FZ to roughly zero in near BMZ due to the variations in cooling rate.

3.3 Microstructure of FZ

The continuous cooling transformation (CCT) curve of Ti-6Al-4V alloy is presented by the schematic diagram in Fig. 5a [16]. It is clearly observed from CCT curve (Fig. 5a) that for achieving fully α' martensitic microstructure, the cooling rate should be above 410 °C/s. Whereas, a massive transformation (α_m) takes place for cooling

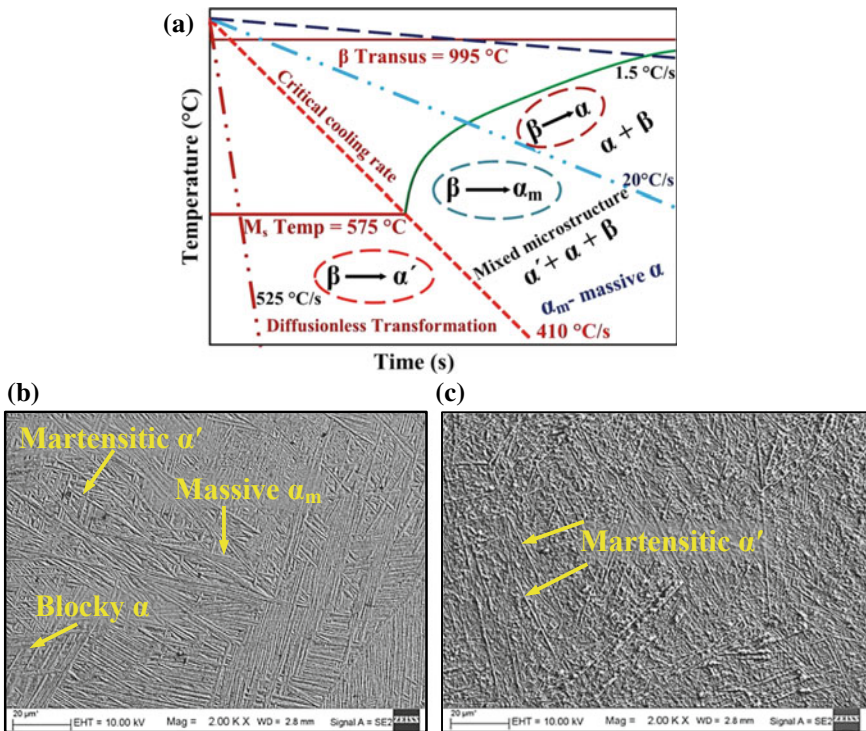


Fig. 5 a Schematic diagram of CCT curve of Ti-6Al-4V alloy [16]; microstructure of FZ for welding speed of b 500 mm/min and c 600 mm/min

rates between 410 and 20 °C. No transformations of β phase into α' phase occur below 20 °C/s cooling rate. The comparative studies of developed microstructures in FZ of weldments are conducted by FESEM micrographs in Fig. 5b–c at two different welding speeds for Exps. 1 and 2.

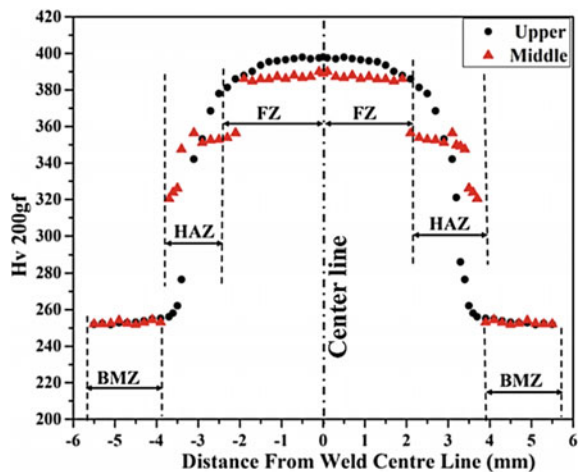
At slowest traverse speed of 500 mm/min, insignificant volume of grain boundary α and massive α_m phases before β grain boundaries is observed in a dominant phase of α' martensite (Fig. 5b). The existence of massive α_m indicates that cooling rate for this combination of process parameters is most likely close to the 410 °C/s for evaluation of martensitic structure (α') in FZ. These observations are fairly agreed with CCT diagram as presented in Fig. 5a for massive transformation as reported in the literature [16].

In Fig. 5b–c, it is also observed that with increased LBW speed at a beam power of 1100 W, the thickness and size of needle-shaped lamella of α' martensite is reduced. With an increase of welding speed, the cooling rate of fusion area is also increased due to the reduction of interaction time of laser beam with the base metal and it enhances the nucleation rate of new colonies of α' lamellae on both β -phase boundaries and within β grains. Consequently, at higher cooling rate the β -phase is fully converted into α' martensitic structure in diffusion less manner. Therefore, fully α' martensitic structure is formed from the prior β grains in sample of Exp. 2 as shown in Fig. 5c. These microstructural studies in Fig. 5b–c clearly reveal that the LBW process has characteristics of high self-quenching rate.

3.4 Microhardness

The Vickers microhardness distribution curve of the welded sample of Exp. 2 (Table 3) is presented in Fig. 6. The hardness values are measured at upper and

Fig. 6 Vickers hardness profile for Exp. 2 (Table 3)



middle part of weld bead across transverse direction of the weld line. The lowest value of hardness is found in BMZ. The hardness increases continuously from BMZ to within HAZ (near FZ boundary). Further, the hardness value reaches to its highest point in the FZ due to the existence of harder α' martensite which possesses high hardness. The amount of α' martensitic phase reduces from approximately hundred percent in FZ to approximately zero percent in BMZ. Subsequently, hardness is also reduced on both the side of center line of FZ (Fig. 6). It is also observed in Fig. 6 that the hardness at the top side of bead are higher than the middle section due to faster cooling of top portion as it is in contact with surrounding atmosphere. Faster cooling rate enhances the formation of coarser to finer lamella of α' martensite. The finer α' lamella is very hard and brittle in nature and shows high hardness.

4 Conclusions

In the present study, a continuous wave 2 kW fiber laser is used to explore the quality of weldments of Ti-6Al-4V alloy plates. The weld surface is efficiently shielded by providing argon gas. Smooth and uniform beads with crack-free weldments are formed. Microstructure variations are found from fusion zone to heat-affected zone due to the changes in cooling rate. α' martensitic structure is found in both fusion zone and near heat-affected zone. Also, the different morphologies of α' martensitic phase such as massive α_m and transformed α are found in fusion zone. The % of α' martensitic phase is reduced from about 100% in the fusion zone to nearly zero in base metal zone. Maximum hardness is found in fusion zone of the weld bead due to the development of large volume of martensitic α' .

References

1. Donachie, M.J.: Titanium: a Technical Guide, 2nd edn. ASM International, Materials Park, OH (2000)
2. Leyens, C., Peters, M.: Titanium and Titanium Alloys: Fundamentals and Applications. Wiley-VCH Verlag GmbH & Co. KGaA, Weinheim, FRG (2003). <https://doi.org/10.1002/3527602119>
3. Li, Zhang, Gobbi, S.L., Norris, I., Zolotovskiy, S., Richter, K.H.: Laser welding techniques for titanium alloy sheet. J. Mater. Process. Technol. **65**(1–3), 203–208 (1997). [https://doi.org/10.1016/S0924-0136\(96\)02263-7](https://doi.org/10.1016/S0924-0136(96)02263-7)
4. Assuncao, E., Quintino, L., Miranda, R.: Comparative study of laser welding in tailor blanks for the automotive industry. Int J Adv Manuf Technol **49**(1–4), 123–131 (2010). <https://doi.org/10.1007/s00170-009-2385-0>
5. Ayoola, W.A., Suder, W.J., Williams, S.W.: Parameters controlling weld bead profile in conduction laser welding. J. Mater. Process. Technol. **249**, 522–530 (2017). <https://doi.org/10.1016/j.jmatprotec.2017.06.026>
6. Wang, S., Wei, M., Tsay, L.: Tensile properties of LBW welds in Ti–6Al–4V alloy at evaluated temperatures below 450 °C. Mater. Lett. **57**(12), 1815–1823 (2003). [https://doi.org/10.1016/S0167-577X\(02\)01074-1](https://doi.org/10.1016/S0167-577X(02)01074-1)

7. Squillace, A., Prisco, U., Ciliberto, S., Astarita, A.: Effect of welding parameters on morphology and mechanical properties of Ti-6Al-4V laser beam welded butt joints. *J. Mater. Process. Technol.* **212**(2), 427–436 (2012). <https://doi.org/10.1016/j.jmatprotec.2011.10.005>
8. Caiazzo, F., Alfieri, V., Corrado, G., Cardaropoli, F., Sergi, V.: Investigation and optimization of laser welding of Ti-6Al-4V titanium alloy plates. *J. Manuf. Sci. Eng.* **135**(6), 61012–61018 (2013). <https://doi.org/10.1115/1.4025578>
9. Gursel, A.: Crack risk in Nd: YAG laser welding of Ti-6Al-4V alloy. *Mater. Lett.* **197**(15), 233–235 (2017). <https://doi.org/10.1016/j.matlet.2016.12.112>
10. Costa, A., Miranda, R., Quintino, L., Yapp, D.: Analysis of beam material interaction in welding of titanium with fiber lasers. *Mater. Manuf. Process.* **22**(7–8), 798–803 (2007). <https://doi.org/10.1080/10426910701446671>
11. Kabir, A.S.H., Cao, X., Medraj, M., Wanjara, P., Cuddy, J., Birur, A.: Effect of welding speed and defocusing distance on the quality of laser welded Ti-6Al-4V. *Mater Sci Technol* 2787–97 (2010)
12. Casalino, G., Mortello, M., Campanelli, S.L.: Ytterbium fiber laser welding of Ti6Al4V alloy. *J. Manuf. Process.* **20**(1), 250–256 (2015). <https://doi.org/10.1016/j.jmapro.2015.07.003>
13. Ahn, J., Chen, L., Davies, C.M., Dear, J.P.: Parametric optimisation and microstructural analysis on high power Yb-fibre laser welding of Ti-6Al-4V. *Opt. Lasers Eng.* **86**, 156–171 (2016). <https://doi.org/10.1016/j.optlaseng.2016.06.002>
14. Gao, X.L., Zhang, L.J., Liu, J., Zhang, J.X.: Effects of weld cross-section profiles and microstructure on properties of pulsed Nd: YAG laser welding of Ti6Al4V sheet. *Int. J. Adv. Manuf. Technol.* **72**(5–8), 895–903 (2014). <https://doi.org/10.1007/s00170-014-5722-x>
15. Geels, K., Kopp, W., Ruckert, M.: Metallographic and materialographic specimen preparation, light microscopy, image analysis, and hardness testing. *Manual* **46** (2006)
16. Ahmed, T., Rack, H.J.: Phase transformations during cooling in $\alpha + \beta$ titanium alloys. *Mater. Sci. Eng. A* **243**(1–2), 206–211 (1998). [https://doi.org/10.1016/S0921-5093\(97\)00802-2](https://doi.org/10.1016/S0921-5093(97)00802-2)